The J-Index: An Integrated Framework for Early Breast Lesion Identification

Integrating Physics-Based Morphological Reconstruction with Independent Physiological Evidence

Abstract

Breast cancer is the most frequently diagnosed cancer in women worldwide. Its outcomes and treatment are strongly influenced by the stage of tumor development at diagnosis, making early detection central to reducing its human and economic impact. Noninvasive Spatial Thermal Imaging (STI) was developed to address this need by identifying and characterizing suspicious subsurface lesion morphology during early tumor development.

STI uses a conventional thermal breast image as input. Unlike conventional breast thermography, which interprets the diffusion-broadened surface pattern directly, STI treats the surface field as data for inverse reconstruction. Pixel-by-pixel heat-transfer analysis is used to recover underlying morphology, while wavelet analysis provides multiscale support for reconstructed characteristics. These findings form the Morphology Index (M-Index). A separate Physiological Index (P-Index) characterizes macroscopic surface physiology, and the independently derived indices are integrated to form the J-Index.

STI is intended for primary breast screening. Its spatial resolution has enabled reconstruction of suspicious morphology at dimensions compatible with early tumor development, including one illustrative case in which a model-derived 2 mm width corresponded to a 2 mm pathological measurement. Prospective validation is required to establish diagnostic performance.

Keywords: breast imaging; thermal imaging; inverse heat transfer; morphological reconstruction; breast cancer screening

1. Introduction

Breast cancer, the most frequently diagnosed cancer in women worldwide,[1] imposes a burden extending well beyond mortality, including treatment-related morbidity, lasting physical and cognitive effects, impaired quality of life, disfigurement, and substantial economic cost. Because both survival and treatment are strongly influenced by tumor development at diagnosis, earlier malignancy detection remains central to reducing the human and economic consequences of the disease. 2

Spatial Thermal Imaging (STI) was developed to address this need by reconstructing and characterizing suspicious subsurface lesion morphology during early tumor development.

Conventional breast thermography (BT) characterizes physiological abnormality from qualitative and quantitative features observed directly in the surface thermal field. The J-Index framework retains this established form of surface physiological assessment as the Physiological Index (P-Index). STI, however, constitutes a separate analytical process: rather than interpreting the

surface thermal pattern, it applies inverse heat-transfer reconstruction to recover the subsurface morphology responsible for the measured field. A physiologically low-risk surface classification, however, cannot exclude a small, deep, or otherwise weakly expressive lesion because the measured surface field represents a diffusion-broadened manifestation of underlying heat sources rather than a direct image of subsurface morphology. Accordingly, a physiologically reassuring surface examination and a morphologically suspicious subsurface lesion are not mutually exclusive. STI addresses this limitation by reconstructing the subsurface morphology responsible for the measured surface field rather than by refining interpretation of the surface thermal pattern.

Early tumor development may remain constrained during a diffusion-limited avascular phase. [3] As cellular expansion produces hypoxia, HIF-1α-mediated expression of vascular endothelial growth factor and other proangiogenic signals may initiate the angiogenic switch.[4] Acquisition of a supporting microvascular network can then permit transition from microscopic dormancy or slow growth to substantially more rapid expansion.[5] Conventional structural imaging performs well once sufficient anatomical change has developed to permit direct lesion characterization, but this requirement creates an interval during which pathological development may be underway before the responsible lesion becomes directly distinguishable. This interval provides the biological rationale for reconstructing clinically meaningful subsurface lesion morphology from the measured surface thermal field before conspicuous anatomical or physiological expression develops.

Unlike analytical methods that attempt to derive morphology directly from the diffusion-broadened surface thermal pattern, STI evaluates each recorded pixel and its adjoining pixels as solutions of the heat equation and applies pixel-by-pixel inverse heat-transfer reconstruction to recover the subsurface heat-generating morphology responsible for the observed field. This approach accounts for diffusion-induced broadening rather than attempting to reproduce the distorted surface projection directly. Once reconstruction has been performed, the diffusion profile itself becomes a source of spatial information: full width at half maximum measurements, together with spatial thermal gradients and related field characteristics, are used to estimate lesion dimensions, depth, and surrounding tissue properties.

Reconstructed lesion morphology is evaluated for structural and vascular characteristics associated with pathological processes.[6-10] Wavelet analysis[11] assesses the multiscale coherence and persistence supporting each identified characteristic and modulates its contribution to the Morphology Index (M-Index). The M-Index therefore represents the pathological implication supported by the reconstructed lesion morphology.

The present framework assigns conventional thermography a narrow physiological role. Examinations are acquired under a defined protocol that controls influences capable of altering the surface thermal field. Physiological interpretation is based on predefined vascular observations and quantitative bilateral and regional temperature relationships. The resulting Physiological Index (P-Index) is used solely to characterize the degree of macroscopic physiological activity expressed at the breast surface—information analytically distinct from, and not contained within, the reconstructed morphology represented by the M-Index. Accordingly, an elevated P-Index may provide corroborating physiological evidence, whereas a

low P-Index cannot exclude a small, deep, or weakly expressive lesion and must not negate strongly supported reconstructed morphology.

The J-Index was developed to combine these complementary morphological and physiological evidence streams within a single reporting framework while preserving the independent derivation and contribution of each. Because the two indices characterize different manifestations of disease, concordance is not required; a morphologically suspicious lesion may exhibit little surface physiological expression, while physiological abnormality may occur without corresponding suspicious localized morphology. The J-Index retains these distinctions rather than permitting either component to substitute for the other.

This paper describes the physics-based reconstruction of lesion morphology; its characterization through the M-Index; the independent physiological assessment represented by the P-Index; and their integration within the J-Index framework.

2. Thermodynamic Framework of Morphological Reconstruction

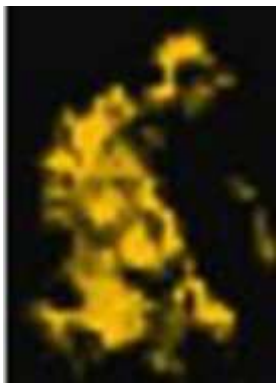

Figure 1. Representative STI morphological reconstruction illustrating recovery of thermal morphological fine structure. The reconstructed morphology demonstrates spatial organization, irregular geometry, and structural occupancy of the underlying heat-generating structures, providing the basis for subsequent quantitative morphological characterization.

The thermodynamic principles underlying Subsurface Tissue Imaging (STI) are based on the physics of heat generation and diffusion within biological tissue.[12] Localized metabolic activity and angiogenic vascular recruitment associated with pathological development may produce spatially confined thermal fields within breast tissue. Heat generated by these internal sources propagates through surrounding tissue and contributes to measurable temperature distributions at the skin surface.

The measured surface thermal field does not constitute a direct image of the originating subsurface source. Rather, it represents a diffusion-transformed projection shaped by tissue thermal properties, vascular perfusion, source geometry, propagation distance, and boundary heat exchange. STI treats this measured field as thermodynamic data from which surviving spatial information concerning the underlying heat-source distribution can be reconstructed.

Heat Propagation and Diffusion Effects

Heat generated within biological tissue propagates through conductive diffusion, with vascular perfusion and other tissue properties modifying the resulting thermal field. As thermal energy travels from a subsurface source toward the skin surface, the spatial temperature distribution broadens because of diffusion and tissue heterogeneity. Consequently, fine spatial detail associated with the originating source becomes attenuated while lower-frequency spatial organization may remain detectable at the surface.

From an imaging perspective, this diffusion-induced broadening may be approximated as a convolution between the subsurface heat-source distribution and the thermal point-spread behavior of intervening tissue. Thermal diffusion therefore acts as a spatial low-pass process that attenuates high-frequency spatial variation while preserving broader spatial relationships within the measured field.

STI interprets the surface thermal image as a set of boundary observations arising from this diffusion process. Inverse analysis is then applied pixel by pixel to estimate the spatial morphology and organization of the heat sources responsible for the measured surface temperature distribution. The reconstruction does not presume that diffusion preserves an undistorted image of the originating source, nor does it claim to recreate information absent from the measured field. Rather, STI is based on the premise that the diffusion-broadened surface distribution retains low-amplitude, spatially coherent information concerning source location, geometry, and organization that can be recovered through inverse analysis.

Conceptual Visualization: Virtual Thermal Wavefronts

For purposes of conceptual development, STI treats thermal patterns as virtual thermal wavefronts associated with heat flow from localized subsurface physiological sources.[13] The virtual-wave concept is used solely as an interpretive visualization framework and does not replace the underlying diffusion-based thermodynamic formulation.

Within this conceptual model, the temperature associated with each recorded pixel represents a local expression of heat propagation from an underlying source.[14] This visualization provides an intuitive means of relating measured surface temperature patterns to subsurface heat-flow organization while preserving the governing interpretation of heat transfer as a diffusion process.

By reverse modeling the heat flow measured at the breast surface,[15] STI reconstructs the spatial morphology and organization of subcutaneous thermal sources associated with pathological development. This thermodynamic interpretation forms the basis of the reconstruction methodology described below.

3. Morphological Reconstruction Methodology

Heat generated by subsurface tissue reaches the breast surface after transport through tissue having finite thermal conductivity, density, specific heat, vascular perfusion, tissue composition, geometry, propagation distance, and boundary heat-loss characteristics. In a complete bioheat-transfer formulation, these variables jointly determine the relationship between the temperature of the originating heat source and the temperature measured at the skin.

STI does not attempt to estimate each contributing variable independently from a routine thermal examination. Instead, their combined influence is represented through a reduced operational transfer relationship.

In a complete bioheat-transfer formulation, such as the Pennes bioheat equation, tissue temperature is determined by the combined effects of thermal conduction, tissue heat capacity, blood perfusion, metabolic heat generation, internal heat sources, geometry, and boundary conditions. STI does not attempt to solve this full formulation using patient-specific estimates of each contributing variable.

For purposes of the STI reconstruction algorithm, the source-to-surface relationship is represented operationally in reduced form as:

$$T_1 = K * T_0$$

with

$$K = f(\lambda_1, \lambda_2, \ldots, \lambda_n)$$

where T_1 is the surface temperature represented by the recorded pixel, T_0 is the estimated temperature associated with the corresponding subsurface heat-generating source, and K is an effective transfer function representing the cumulative influence of the variables governing source-to-surface heat transfer along the local heat-flow path. This expression is an operational reconstruction relationship rather than a constitutive equation for tissue heat transfer.

The λ_i collectively represent the relevant thermophysical, physiological, geometric, and boundary-condition variables, including tissue thermal conductivity, density, specific heat, perfusion, tissue composition, path length, source geometry, diffusion, and surface heat exchange. STI does not interpret K as a single physical tissue constant. Rather, K functions as a lumped operational representation of the combined transfer conditions between a subsurface source and the measured surface temperature.

This reduced representation does not imply that the individual thermophysical or physiological variables are identical among patients or spatially uniform within the breast. The reduced relationship is not intended as a replacement for the Pennes bioheat equation or as an exact constitutive description of tissue heat transfer. Rather, it is an operational abstraction used by STI to represent the combined effect of variables that cannot practicably be measured independently during routine thermal imaging.[12]

Parameterization and Control of K

Within the STI reconstruction framework, K is parameterized along an ogival response curve. The approximately linear central region of this curve serves as the operational reconstruction domain. Two controls permit variation of K within this domain during developmental, exploratory, and demonstrative reconstruction.

The coarse control establishes an approximate central operating value, while the precision control permits smaller adjustments around that value. The upper and lower operating bounds of these controls were established during early STI development and permanently incorporated into the application.

The purpose of these controls is not to determine a unique physical value of K for an individual patient. Rather, progressive variation permits observation of the range over which coherent structural differentiation is maintained and of the point at which continued adjustment begins to produce fragmentation, loss of edge continuity, and degradation of morphological coherence.

A fixed reconstruction preset within the established operating range was subsequently selected through AI-assisted qualitative comparison of candidate parameter settings. The selected setting preserved coherent structural differentiation while avoiding progressive fragmentation and morphological degradation. This preset was then locked for uniform routine analytical use.

Standardized Reconstruction Workflow

In the standardized analytical workflow, a fixed reconstruction preset is applied to submitted thermal images as the default reconstruction setting. In most examinations, K is not adjusted interactively and no case-specific reconstruction endpoint is selected. In a small subset of examinations, however, image quality may be insufficient for reliable downstream AI analysis when the fixed preset is used. In these cases, the coarse and precision controls may be adjusted within the established operating bounds to improve reconstruction adequacy and permit interpretable morphological analysis.

The resulting reconstruction is used for AI-based lesion identification, localization, morphological characterization, and confidence assessment. Analytical outputs include lesion-identification confidence W, characteristic-specific wavelet confidence values w_i, and the pathological-implication reporting category W_m.

The coarse and precision controls are used primarily for developmental, exploratory, and demonstrative reconstruction, but may also be employed in exceptional examinations in which image quality prevents adequate analysis using the fixed preset. Such adjustments are based on overall reconstruction adequacy and are intended to restore sufficient structural coherence for analysis rather than to optimize or intensify the appearance of a particular lesion. Figures 2 and 2A illustrate the broader behavior of the reconstruction as K is varied. Figure 2 demonstrates progressive structural differentiation, while Figure 2A illustrates the loss of morphological coherence and fragmentation that occurs when adjustment is extended beyond the useful operating domain.

The reduced K representation does not constitute an exact solution of the complete bioheat-transfer problem, nor is K interpreted as a uniquely measurable tissue parameter. It is an operational transfer function used within the STI inverse-reconstruction framework to represent the combined effect of multiple source-to-surface heat-transfer variables. Its purpose is to provide a standardized reconstruction environment based on a fixed analytical preset, with limited adjustment permitted when necessary to obtain an analytically adequate reconstruction from a technically suboptimal image.

The software source code and certain implementation-specific processing routines remain proprietary.

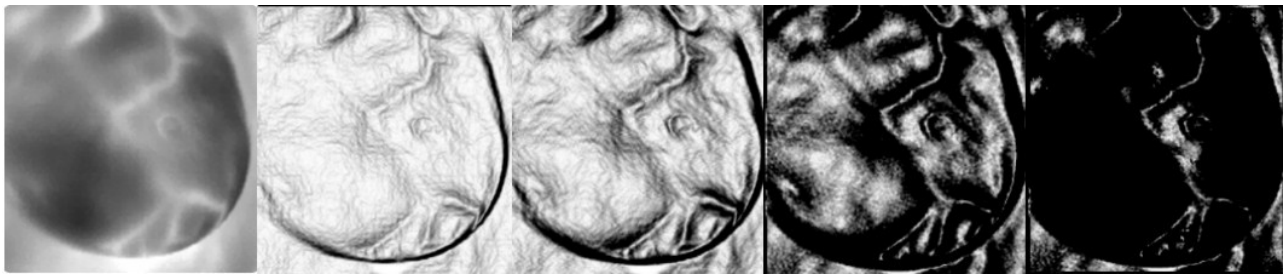

Figure 2. Representative progression of iterative STI morphological reconstruction from the measured surface field (raw thermal image) to a fully developed demonstrative reconstruction.

Successive reconstruction iterations illustrate the progressive differentiation of the recovered morphology as K is varied. The fixed preset used in the standardized screening workflow produces an analytical reconstruction broadly comparable in appearance to Iteration 1, although the correspondence is not exact because Figure 2 illustrates the general reconstruction sequence rather than the processing of a specific screening image. The later iterations demonstrate further development of the visualization for exploratory and demonstrative purposes. Continued adjustment eventually produces loss of edge continuity, fragmentation, and degradation of morphological coherence, as illustrated in Figure 2A.

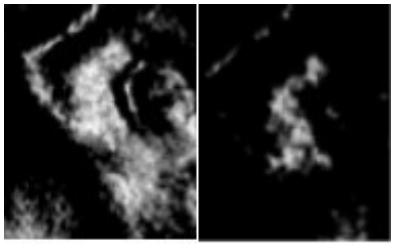

Figure 2A. STI reconstruction endpoint versus K over-adjustment. The optimum reconstruction is shown at left; further increase in K produces fragmentation and loss of morphological coherence, as shown at right. The optimum reconstruction also demonstrates a compact cluster of small hypointense voids within the lesion margin, illustrating the morphology designated C8.

3.1 Geometric Estimation of Reconstructed Heat Sources

The selected reconstructed morphology identifies the presence and structural characteristics of reconstructed heat sources. A complete clinical characterization also requires estimation of their geometric properties. Reconstructed-source dimensions, depth, and surrounding tissue

characteristics provide important contextual information for clinical interpretation and facilitate comparison with other imaging modalities.

Geometric characteristics of reconstructed heat sources may be estimated from the diffusion-modified thermal field produced at the surface by heat originating from vascular or metabolic sources. This surface thermal field can be approximated by a Gaussian diffusion profile, permitting characterization of the spatial thermal distribution by its full width at half maximum (FWHM) and associated gradient properties.

Measurement of the FWHM of the diffusion-broadened thermal field provides an estimate of the lateral dimension of the reconstructed heat source. Additional parameters, including spatial temperature gradients and the relative intensity of principal vascular structures, provide insight into the effective thermal diffusivity of the intervening tissue. Together, these relationships permit approximate estimation of reconstructed-source width, source depth, and surrounding tissue-density characteristics. In the current implementation, depth estimation employs a first-order heuristic relationship between diffusion-profile width and propagation distance, constrained by the estimated thermal characteristics of the intervening tissue. Although this approximation provides useful geometric estimates, the precise functional relationship remains an area of ongoing refinement. [17]

3.2 Resolution Stability of Morphological Reconstruction

Comparable reconstructed morphology has been obtained from thermal images acquired at detector resolutions ranging from approximately 160 × 120 pixels to 640 × 480 pixels. Higher-resolution sensors primarily improve the visual definition of fine vascular and lesion-associated structures rather than materially altering the principal reconstructed morphology. This behavior is consistent with thermal diffusion acting as a spatial low-pass process: the measured surface field contains limited spatial bandwidth, while STI reconstructs the spatially coherent information that remains within that field. Accordingly, meaningful morphological reconstruction can be obtained from relatively low-cost thermal detectors, although formal cross-resolution validation remains necessary.

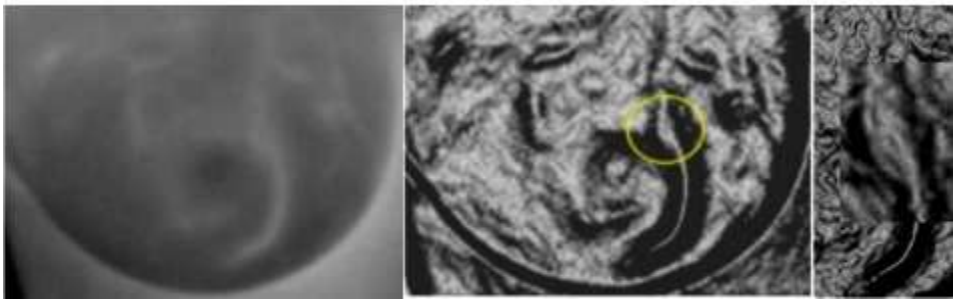

Figure 3. Representative STI reconstruction from a 160 × 120-pixel thermal acquisition.
(A) Original grayscale thermogram. (B) Reconstructed subsurface morphology, with the region of interest indicated. (C) Enlarged view demonstrating fine structural detail within the reconstruction. The reconstructed lesion has a model-derived width estimate of approximately 2 mm based on calibrated image geometry.

4. Morphological Interpretation Framework (M-Index)

The M-Index framework evaluates seven characteristics of reconstructed lesion morphology, designated C2 through C8, together with one independent vascular-association factor, C1. C1 is not itself a morphological characteristic. It represents the biological plausibility that the reconstructed lesion is supported by an anatomically appropriate vascular supply and is therefore applied separately from the morphology-derived contributions. C1 does not add an additional morphological feature; rather, it serves as an independent biological-plausibility gate for final M-Index eligibility.

STI analysis proceeds in two stages: thermodynamic reconstruction of the internal thermal field followed by morphological interpretation of the reconstructed heat-source morphology. The resulting morphological features are evaluated using the indicators described below to assign a Morphology Index (M-Index).

The reconstruction process produces a visualization of reconstructed morphology, including vascular architecture, localized heat-generating structures, lesion geometry, and their spatial organization within the breast. Interpretation then evaluates a set of morphological indicators associated with malignancy. The indicators described below were selected from established descriptions of the morphological characteristics most commonly associated with malignant tumors and adapted for evaluation within the STI reconstruction framework.

Seven morphological characteristics and one vascular-association factor, designated C1–C8, are assessed:

Indicator	Imaging Manifestation	Biological Interpretation or Analytical Role
C1 – Vascular association	Lesion occurs adjacent to or integrated with vascular structures	Biological-plausibility factor
C2 – Focused vascularity	Localized concentration of vessels surrounding a lesion	Angiogenic recruitment
C3 – Thermal state	Hyperthermia/Hypothermia relative to surrounding tissue	Altered local heat generation or transport associated with lesion physiology
C4 – Geometry	Irregular or jagged lesion morphology	Structural disorganization of tumor growth
C5 – Tortuous vessels	Curved, chaotic vascular morphology	Established tumor angiogenesis
C6 – Distorted vessels	Dilated or elongated vessel near lesion	Early vascular remodeling
C7 – Feeder/Drainage pattern	Presence of afferent and efferent vessels	Functional vascular network supporting lesion
C8 – Microthermal bubble formations	Cluster of tiny cyst-like or hypointense bubble structures embedded within or immediately contiguous with the lesion	Possible localized biochemical activity associated with the angiogenic microenvironment

Table 1. Morphological Characteristics and Vascular-Plausibility Factor Used in the M-Index Framework

Among these indicators, three are assigned particular interpretive significance within the current STI hierarchy: irregular geometry indicating structural irregularity of tumor growth (C4), tortuous vascular structures consistent with tumor-associated angiogenesis (C5), and distorted vessels associated with early vascular remodeling (C6).

Microthermal bubble formations (C8) were recognized following retrospective examination of cases initially interpreted as benign cystic structures but later associated with malignant pathology. Their appearance is suggestive of localized nitric oxide-related biochemical activity within the tumor microenvironment. Within the current STI framework, C8 requires a cluster of tiny cyst-like or hypointense bubble structures embedded within or immediately contiguous with the reconstructed lesion. Isolated maxima, paired voids, or spatially separated features are not sufficient for C8 assignment. An example is visible in the optimum reconstruction in Figure 2A, where several discrete rounded hypointense voids, each spanning approximately 3–4 pixels (1.4–1.8 mm at the calibrated image scale) form a compact cluster within the lesion margin. Their biological origin remains under investigation, although they may reflect localized biochemical activity associated with the angiogenic microenvironment.

Each of the seven morphological characteristics, C2–C8, is assigned a maximum heuristic contribution reflecting its relative importance within the STI analytical hierarchy. These contributions represent a working formalization of the qualitative interpretive hierarchy developed through iterative clinical observation and case-based refinement. C1 is treated separately as a variable biological-plausibility gate determined by lesion-to-vessel distance and does not contribute additively to the raw morphology score. As the STI case database expands, empirical calibration of both the morphological contributions and the vascular-association function against outcome-correlated data is anticipated.

Indicator	Diagnostic Role	Weight	Interpretation Role
C1 – Vascular association	Biological plausibility gate	Variable 0-1	Function of lesion-to-vessel distance
C2 – Focused vascularity	Light	1	Local angiogenic recruitment
C8 – Bubble formations	Light	1	Early biochemical activity
C3 – Thermal anomaly	Supportive	1.5	Metabolic activity
C7 – Feeder-Drainage pair	Moderate	2	Functional vascular support network
C4 – Irregular geometry	Heavy	3	Structural irregularity of tumor growth
C5 – Tortuous vessels	Heavy	3	Classic tumor angiogenesis
C6 – Distorted vessels	Heavy	3	Early vascular remodeling

Table 2. Maximum Heuristic Contributions of Morphological Characteristics and the C1 Vascular-Association Gate

The relative interpretive significance of the seven morphological characteristics differs. In the current implementation, each maximum contribution is modulated by wavelet-derived measures of structural coherence and persistence.

Heavy weight (3.0)
C4, C5, and C6 represent the principal structural and angiogenic characteristics within the STI morphological hierarchy. Their combined presence provides the strongest basis for an elevated M-Index assignment. C4 reflects irregular lesion geometry associated with structurally disorganized growth. C5 reflects tortuous vascular architecture consistent with tumor-associated angiogenesis, while C6 reflects vascular distortion associated with early microcirculatory remodeling. Together, these characteristics may support identification of developing lesions before a fully established malignant vascular architecture is present.

Moderate weight (2.0)
C7 reflects the identification of both afferent feeder and efferent drainage vessels associated with

the reconstructed lesion, consistent with an established functional vascular network. Its presence provides significant support within the STI morphological hierarchy but is weighted below the heavy characteristics because a fully developed feeder–drainage pattern may not yet be present in early-stage lesions.

Supportive/Conditional weight (1.5)
C3 represents a thermal anomaly—hyperthermia or hypothermia—relative to surrounding tissue. Marked hyperthermia (≥1 °C) is most commonly associated with inflammatory carcinoma and is absent in the majority of malignant lesions. Hypothermia may occur in slowly growing or weakly expressive lesions. Consequently, the absence of a marked thermal anomaly is not penalizing, while a coherent lesion-associated thermal departure provides conditional support within the morphological assessment.

Light weight (1.0)
C2 and C8 provide supportive evidence but carry reduced standalone interpretive weight because of overlap with benign processes. Focused vascularity may accompany benign cystic or hyperplastic changes. C8 requires a cluster of tiny cyst-like or hypointense bubble structures embedded within or immediately contiguous with the reconstructed lesion; isolated maxima, paired voids, or spatially separated features do not qualify. Although C8 may reflect localized biochemical activity associated with the angiogenic microenvironment, its biological basis and pathological specificity remain under investigation.

Lesion Identification Confidence (W)

Lesion identification confidence, W, is determined from six independently evaluated components describing the reliability of lesion identification and morphological characterization.[18-19] These components are presently heuristic measures subject to future empirical calibration.

$$W = f(E, D, L, B, F, I)$$

where:

- **E** – coherent lesion existence
- **D** – correct dominant-candidate selection
- **L** – lesion-core localization
- **B** – binding of C2–C8 to the identified lesion
- **F** – stability of the reconstructed lesion field and geometric dimensions
- **I** – image adequacy and freedom from confounding influences

Parameter B quantifies the confidence that the reconstructed morphological characteristics C2–C8 are correctly associated with the same identified lesion rather than with an adjacent vessel, unrelated structure, or separate candidate.[20] It evaluates the internal consistency of lesion identification and is independent of C1 vascular association.

For reporting purposes, lesion identification confidence is conveyed qualitatively using the descriptors Minimal, Low, Medium, Medium-High, High, and Maximum rather than as

numerical percentages. These descriptors communicate the relative reliability of lesion identification without implying a statistically calibrated probability.

Having established confidence in lesion identification, the reconstructed morphological characteristics are subsequently evaluated within the STI interpretive framework to determine their collective implication of underlying pathology.

Wavelet-Derived Feature Confidence

Wavelet analysis (WA) is a mathematical methodology for evaluating spatial fields simultaneously across multiple spatial scales. Unlike conventional spatial filtering techniques, wavelet decomposition preserves spatial localization while examining structural organization over several levels of resolution.

Applied to STI, wavelet analysis supports the selection of candidate morphological characteristics C2–C8 and confirms their spatial coherence and persistence across multiple decomposition scales.[21-23] Characteristics that remain spatially coherent and persistent across scales are assigned greater wavelet confidence than isolated, unstable, or scale-dependent features. The normalized wavelet confidence assigned to each characteristic modulates its maximum heuristic contribution to the raw morphology score.

Wavelet analysis assigns a normalized confidence value, w_i, to each reconstructed morphological characteristic C2–C8. Each w_i expresses the confidence that the corresponding characteristic is genuinely present, spatially coherent, and persistent across multiple decomposition scales. These feature-specific confidence values modulate the maximum heuristic contributions used to calculate the raw morphology score. They do not independently determine pathological implication, which is expressed separately by W_m as described below.

Morphology Index Computation

The wavelet-modulated morphological characteristics are evaluated within a weighted interpretive framework to derive the Morphology Index (M-Index), ranging from M0 to M6.[24] The raw morphology score represents the cumulative strength of the seven reconstructed morphological characteristics, C2–C8. C1 vascular association is evaluated separately and does not contribute additively to this score.

Raw Morphology Score Computation

The raw morphology score, S, is calculated as:

$$S = C_2 + C_3 + C_4 + C_5 + C_6 + C_7 + C_8$$

Each wavelet-modulated contribution, Ci, is computed as

$$C_i = 0, \text{ for } w_i < 0.25,$$

$$C_i = w_i C_{i,max}, \text{ for } w_i >= 0.25.$$

where w_i is the normalized wavelet confidence assigned to characteristic C_i, and C_i,max is its maximum heuristic contribution.

The resulting raw score determines the provisional M-Index classification. Final classification remains subject to the independent C1 vascular-association requirement described below.

M-Index Mapping

The raw morphology score is mapped to the M-Index using the following threshold table. These threshold values represent the current operational STI classification and may be refined as additional outcome-correlated data become available.

Score S	M-Index	Description
S = 0	M0	No morphological findings
0 < S <= 2	M1	Minimal morphological findings
2 < S <= 4.5	M2	Moderate morphological findings
4.5 < S <= 7.0	M3	Substantial morphological findings
7.0 < S <= 11	M4	Morphology suspicious for malignancy
11 < S <= 13.4	M5	Morphology strongly suspicious for malignancy
S > 13.4	M6	Morphology highly characteristic of malignancy

Table 3. M-Index Wavelet Confidence-Weighted Classification Thresholds

Pathological Implication Reporting Category, W_m

W_m expresses the qualitative strength of the pathological implication supported by the reconstructed morphology, conditional on the lesion having been correctly identified. It is distinct from lesion identification confidence, W, which evaluates whether the lesion has been reliably identified, selected, localized, and characterized.

W_m is derived solely from the raw morphology score, S. Neither lesion identification confidence, W, nor C1 vascular association modifies W_m . C1 remains an independent biological-plausibility requirement for final M-Index eligibility.

Wm is reported qualitatively according to the strength of S. These qualitative descriptors communicate the relative strength of the pathological implication supported by the reconstructed morphology without implying a statistically calibrated probability. For reporting purposes, Wm is expressed as Minimal, Low, Moderate, Elevated, High, or Very high.

Individual morphological characteristics contribute to the raw morphology score according to their wavelet-modulated values. However, only characteristics whose normalized wavelet confidence, w_i, equals or exceeds 0.25 are cited individually in the narrative justification. Characteristics below this threshold are excluded from the raw morphology score and are not cited as supporting the reported pathological implication.

C1 Vascular-Association Gate

C1 provides an independent assessment of biological plausibility based on the spatial relationship between the reconstructed lesion and an anatomically appropriate vascular structure. It does not contribute to the raw morphology score, S, and does not modify W_m. Consequently, the characteristics C2–C8 may produce both a high raw morphology score and high pathological implication reporting confidence even when vascular association is weak or absent.

C1 does not require a mature tumor-specific vascular architecture or an established feeder–drainage network. It requires only sufficient spatial association with an anatomically plausible existing or recruited vascular structure to support biological viability; therefore, an early lesion may satisfy C1 while lacking C7 and other manifestations of developed angiogenesis.[25] The C1 threshold is intended to reject structurally coherent mimics that are spatially uncoupled from plausible vascular support, not to exclude lesions that have not yet developed a mature angiogenic network.

C1 is determined from the shortest lesion-to-vessel separation and decreases exponentially as that distance increases.[26] Within the current STI implementation, a C1 value below 0.25 indicates insufficient vascular association to support an M1-or-higher classification. This threshold marks the lesion-to-vessel separation at which vascular association falls below the minimum biological-plausibility criterion of the current STI model.

The final M-Index classification is therefore determined as follows:

$$M_{\text{final}} = \begin{cases} M0, & C1 < 0.25, \\ M_{\text{provisional}}, & C1 \geq 0.25. \end{cases}$$

When $0 \leq C1 < 0.25$, the final classification is M0 regardless of the raw morphology score or W_m. This result does not mean that the reconstructed morphology is absent or unreliable. Rather, it indicates that morphology potentially associated with malignancy may have been identified with high structural confidence but lacks sufficient vascular association to satisfy the biological-plausibility requirement of the STI framework. Such morphology may occur in nonmalignant processes, including fibrocystic or hyperplastic tissue changes.

For reporting purposes, C1 vascular association is described qualitatively as:

- $0.75 \leq$ C1 ≤ 1.0: strong vascular association
- $0.50 \leq$ C1 < 0.75: probable vascular association
- $0.25 \leq$ C1 < 0.50: possible vascular association
- $0 \leq$ C1 < 0.25: insufficient vascular association

This keeps the three functions separate:

S = strength of the morphology

W_m = confidence in its pathological implication

C1 = biological eligibility for an M1-or-higher

Limitations and Future Calibration

The maximum heuristic contributions assigned to C2–C8, the M-Index threshold boundaries, and the qualitative confidence mappings used for W and W_m represent current operational parameters developed through iterative clinical observation and case-based refinement. They have not yet been empirically calibrated using population-level outcome data. The C1 vascular-association threshold is informed by published pathological observations concerning lesion-to-vessel separation but likewise requires prospective validation within the STI framework.

The fixed reconstruction preset was selected qualitatively from three candidate reconstructions of a single representative image. Its optimality and generalizability have not been established and require evaluation across a larger, outcome-correlated image set.

Wavelet-derived confidence modulation reduces reliance on binary feature assignment by scaling each maximum heuristic contribution according to the multiscale coherence and persistence of the reconstructed characteristic. It therefore provides a bridge between purely heuristic weighting and future statistically optimized parameter estimation, but does not independently validate the assigned contributions or M-Index threshold boundaries. This developmental pathway is consistent with the historical evolution of many clinical scoring instruments. For example, the ACR BI-RADS[27] lexicon originated as an expert-consensus classification system before undergoing subsequent prospective epidemiological validation.

The mathematical framework is structured to support prospective calibration. As outcome-correlated data accumulate, statistical modeling approaches, including logistic regression or likelihood-ratio analysis, may be applied to estimate the relative contribution of each characteristic and refine the classification thresholds for the intended screening population.

Until such calibration is completed, M-Index values should be interpreted as operational classifications within the STI analytical framework rather than as statistically calibrated probabilities of malignancy, consistent with the current experimental status of STI.

5. Physiological Interpretation Framework (P-Index)

The Physiological Index (P-Index) provides an independent assessment of the macroscopic physiological activity expressed by the breast. The P-Index considers physiological manifestations associated with malignant development, including vascular activity, metabolic response, tissue remodeling, and other thermophysiological indicators observable within the surface thermal field. Together, lesion morphology and the accompanying physiological response provide complementary information about the pathological process expressed within the breast.

The thermal breast image used for morphological reconstruction provides the data required to assess the physiological behavior of the breast using conventional breast thermography, although the P-Index uses a modified implementation. Conventional physiological thermography is limited as a lesion-detection method because it may yield either no detectable signal or unresolved interpretive ambiguity. Early, weakly expressive lesions may not produce sufficient thermal expression at the breast surface to be reliably distinguished, and when surface abnormalities are present, they may also resemble patterns produced by benign physiological or inflammatory processes.

Physiological Indicators

Gautherie[28] evaluated approximately 175,000 symptomatic women using breast thermography and developed an objective thermophysiological classification system in which clearly abnormal thermal patterns were associated with increased breast-cancer risk. His principal interest was the prognostic significance of abnormal thermal images rather than exclusion of disease by normal, borderline-normal, or equivocal images. His studies demonstrated a strong association between clearly abnormal thermographic images and subsequent breast-cancer risk.

The STI modified implementation of Gautherie's methodology comprises five qualitative thermopathological indicators and ten quantitative indicators. The qualitative indicators include assessment of vascular-pattern manifestations, while the quantitative indicators represent measurable temperature differences associated with the qualitative observations. The resulting P-Index implementation therefore describes characteristic physiological patterns observed in normal, inflammatory, and pathological breast tissue.

STI addresses identification and characterization of suspicious subsurface lesion morphology during early tumor development. At this early stage, physiological expression may be minimal and may remain unrecognized by conventional thermography. Consequently, low-risk and equivocal physiological classifications do not contribute weight to the combined J-Index; only clearly abnormal physiological findings contribute additional corroborative weight. The P-Index therefore retains the epidemiological association between physiological thermographic abnormality and breast-cancer risk while remaining analytically separate from STI-derived morphology within the J-Index framework.

Thermal Score and P-Index Classification

Each thermopathological indicator contributing to the overall physiological assessment carries a score according to its frequency of occurrence and pathological significance. The total thermal score is obtained by summing the contributions of the qualitative and quantitative indicators

present within the examination. The resulting score is classified into five ordinal physiological categories, shown in Table 4.

P-Index	Image Classification	Thermographic Risk Classification
P1	Physiologically Normal	No Risk
P2	Borderline Normal	Low Risk
P3	Equivocal	Equivocal Risk
P4	Abnormal	High Risk
P5	Severely Abnormal	Extremely High Risk

Table 4. P-Index Physiological Classification Categories

Within the J-Index framework, the P-Index is deliberately asymmetric. P1–P3 do not contribute to the J-Index because normal, low-risk, and equivocal surface physiological findings are inherently ambiguous with respect to the pathological implication of an underlying lesion; P4 and P5, by contrast, provide additional corroborative physiological weight to the combined assessment. The P-Index is not used to detect or localize a lesion; it contributes independent evidence of macroscopic physiological activity when such activity is sufficiently developed to be expressed at the breast surface.

6. J-Index Computation

Analytical Distinction and Complementarity of the M-Index and P-Index

STI is analytically distinct from conventional breast thermography. The J-Index deliberately integrates STI-derived morphology with a separately derived thermographic physiological component.

The M-Index and P-Index are derived through separate computational pathways and characterize different properties of the same breast thermal examination. They are therefore analytically distinct but are not expected to be statistically independent, because the same underlying pathological process may influence both reconstructed morphology and physiological expression. The value of combining the indices arises from discordant examinations in which one evidence stream is elevated while the other is not.

The **M-Index** characterizes local spatial morphology reconstructed from the thermal field, including vascular architecture, thermal gradients, and lesion geometry within specific regions of interest.

The **P-Index** characterizes the global surface thermal field, reflecting macroscopic physiological expression through vascular patterns and bilateral and regional temperature relationships. Because the J-Index represents the combined breast assessment rather than lesion morphology alone, a P4 or P5 classification may elevate the J-Index even when the M-Index is low or absent;

such elevation reflects physiological abnormality and does not imply localization of a lesion by thermography.

This analytical complementarity supports integration of the M-Index and P-Index within a combined framework rather than treating either as a substitute for the other.

The combined J-Index classification, J(p,m), is defined by the lookup matrix shown in Table 5.

Let $m \in \{0,1,2,3,4,5,6\}$ denote the morphological M-Index level, and let $p \in \{1,2,3,4,5\}$ denote the physiological P-Index level. The combined J-Index classification, J(p,m), is:

P/M	M0	M1	M2	M3	M4	M5	M6
P1	Minimal	Minimal	Minimal	Moderate	Elevated	High	Very high
P2	Minimal	Minimal	Minimal	Moderate	Elevated	High	Very high
P3	Minimal	Minimal	Minimal	Moderate	Elevated	High	Very high
P4	Low	Moderate	Elevated	High	High	High	Very high
P5	Low	Elevated	High	High	High	High	Very high

Table 5. J-Index Interpretation Matrix

The J-Index classification comprises an ordered six-level risk scale:

J = {Minimal, Low, Moderate, Elevated, High, Very high}

Boundary Conditions

The Very high classification represents the upper boundary condition of the J-Index:

J(p,6) = Very high for all p.

The M6 classification represents a complete malignancy-associated morphological profile and therefore produces the maximum J-Index classification regardless of the P-Index level. This reflects the clinical principle that a complete malignancy-associated spatial morphology constitutes the highest risk classification independent of global thermal field characteristics.

Properties of the J-Index Matrix

Several structural properties of the matrix are worth noting:

Monotonicity

The function J(p,m) is monotonically non-decreasing in both arguments. Increasing either the M-Index or the P-Index cannot reduce the resulting J-Index classification. It therefore follows that the J-Index constitutes an order-preserving integration of independent morphological and physiological evidence, ensuring that additional evidence from either domain cannot reduce the overall risk classification.

Asymmetric Sensitivity

The matrix is intentionally more sensitive to increases in the **M-Index** than to increases in the **P-Index** at lower morphological levels.

A low M-Index is not disproportionately elevated by a high P-Index. For example, a **P5/M1** combination yields **Elevated** rather than High risk. This reflects the principle that abnormal surface thermal fields alone, without confirmable spatial morphological findings, do not constitute definitive evidence of malignancy.

Conversely, a high M-Index is not disproportionately suppressed by a low P-Index. For example, **P1/M4** produces **Elevated** risk. This reflects the principle that high-confidence focal malignancy-associated morphology carries independent clinical significance even when the global thermal field appears relatively normal.

P5 Floor Effect

At P4 or P5, even M0 produces Low rather than Minimal risk. This reflects the established association between clearly abnormal physiological thermographic images and increased breast-cancer risk.

M6 Ceiling

The Very high condition is reached exclusively through the M6 condition, reinforcing the clinical distinctiveness of a complete malignancy-associated morphological profile.

J-Index	Clinical Interpretation
Minimal	Combined findings do not support further investigation on thermal grounds alone
Low	Combined findings are mildly concerning; routine follow-up
Moderate	Combined findings warrant clinical attention; correlation with other imaging modalities recommended
Elevated	Combined findings are significantly concerning; prompt clinical evaluation is indicated
High	Combined findings are strongly suggestive; urgent clinical evaluation and additional imaging are recommended
Very high	Combined findings represent the highest thermal risk level; immediate clinical evaluation is indicated

Table 6. Clinical Interpretation of J-Index Levels

These interpretations are intended to assist the referring clinician and do not constitute a diagnosis. The J-Index, like the M-Index and P-Index individually, represents an operational classification within the STI analytical framework, consistent with the current experimental status of STI.

For practical clinical reporting, the combined outcome of the M-index, P-index, and J-index is expressed using a compact notation.

Notation

The combined assessment for any submitted case is expressed in the compact notation, e.g., P4/M4/High; P3/M6/Very high.

This notation provides a complete three-dimensional summary of the STI assessment in a compact, unambiguous format suitable for clinical reporting and database management.

Relationship to Prior Combined Indices

The J-index is conceptually related to prior attempts to combine surface thermographic classification with spatial imaging findings but differs in two important respects.

First, the M-Index is derived from a formalized multi-characteristic spatial analysis rather than from qualitative observer impression alone.

Second, the independence of the two inputs is structurally enforced. The P-Index is explicitly excluded from M-Index computation, preventing the double-counting that can occur when

physiological thermal characteristics influence both physiological and morphological scoring simultaneously.

This separation ensures that physiological field interpretation and spatial morphological analysis remain analytically distinct components of the STI analytical framework.

Use of Artificial Intelligence

Artificial intelligence is incorporated into the STI analytical workflow for lesion identification, localization, morphological characterization, and confidence assessment. Final methodological design, scoring architecture, interpretive rules, and reporting criteria remain author-defined.

Generative artificial-intelligence tools, including OpenAI ChatGPT, Anthropic Claude, and Google Gemini, were also used during manuscript development for language refinement, structural review, consistency checking, and critical evaluation of methodological exposition. All scientific claims, methodological decisions, interpretations, and final manuscript content were reviewed and approved by the author. Generative AI was not used to create or modify underlying clinical data.

7. Representative Clinical Report

The following illustrative example demonstrates the style and content of a representative report generated by the STI J-Index framework. It demonstrates how physiological assessment, reconstructed morphological findings, lesion identification confidence, pathological implication reporting confidence, and the combined J-Index classification are integrated into a concise, clinically interpretable report.

Example 1. Representative STI J-Index Report Excerpt. Combined Assessment: P2/M4/Elevated

Left Breast Physiology: (P2) An atypical vascular pattern is seen at the upper half. It is concentrated at the upper-outer quadrant. Its maximum temperature is moderately higher (2.0°C) than the temperature of the same area on the opposite right breast, and mildly higher (1.0°C) than the mean temperature of the same left breast. The left breast is seen with global hyperthermia relative to the temperature of the adjacent sternal region. The temperature of the nipple/areola region of the left breast is significantly higher (1.5°C) than the temperature of the nipple/areola region of the right breast, and moderately higher (1.5°C) than the mean temperature of the same left breast.

Left Breast Morphology: (M4) Internal visualization of the left breast demonstrates a lesion with significant morphological findings (possible malignancy) in the upper-outer quadrant at 1 o'clock, 23 mm from the nipple. The lesion has model-derived estimates of 2.4 mm in width, 3.1 mm in height, and 1.8 cm deep, in medium-density tissue. This lesion demonstrates five of seven morphological signs associated with pathological implication, together with strong vascular association. Two additional morphological characteristics were observed but were insufficient to support the reporting criteria. Confidence in lesion identification is high. Confidence in the

pathological implication of the lesion is elevated. The location of this lesion corresponds with the patient's reported symptom.

Longitudinal Follow-up of Small Lesions

For reconstructed lesions assigned an M2 or M3 morphological classification with model-derived dimensions of 5 mm or less, the STI reporting system specifies shortened reassessment intervals according to lesion size and morphological classification. Repeat examinations are evaluated for interval change in reconstructed lesion dimensions and for changes in the presence, strength, or organization of morphological characteristics C2–C8. These intervals constitute an operational STI surveillance protocol intended to permit recognition of early morphological evolution and are not presented as validated clinical management guidelines.

Future Development and Conclusions

The methodology presented here establishes a physics-based analytical framework for reconstructing, characterizing, and interpreting breast thermal fields. Although the underlying architecture has been established, several components, including wavelet-derived confidence modulation, the maximum heuristic contributions assigned to C2–C8, the M-Index classification thresholds, the C1 vascular-association criterion, and the J-Index matrix assignments, remain subject to empirical calibration and prospective validation. The modular architecture of the framework permits refinement of these individual components without altering its fundamental structure.

Future development will focus on empirical calibration using outcome-correlated data, including refinement of wavelet-derived confidence modulation, estimation of the relative contributions of the morphological characteristics, evaluation of the C1 vascular-association threshold, and prospective optimization of the M-Index and J-Index classifications.

The next stage of STI development will consist of prospective clinical evaluation to determine sensitivity, specificity, predictive value, reproducibility, and clinical utility for early breast-lesion identification. Such evaluation will require collaboration with clinical investigators and appropriately designed patient cohorts incorporating systematic reference-standard follow-up.

Comparable reconstructed morphology has been observed across clinically relevant thermographic image resolutions. This apparent resolution stability suggests that STI implementation may not require specialized high-resolution instrumentation. Conventional breast-thermography systems, including relatively low-cost thermal cameras already used in clinical imaging practices, may therefore provide a practical foundation for prospective evaluation and future implementation of the J-Index framework.

In summary, the STI/J-Index framework combines inverse thermodynamic reconstruction of breast thermal fields with structured morphological and physiological interpretation. The present report defines the analytical architecture, operational classification system, and observational basis of the method; it does not establish diagnostic performance. STI and the J-Index are presented as developed but not yet prospectively validated analytical methods for reconstructing

and integrating morphological and physiological information from breast thermal imaging. Prospective studies incorporating systematic reference-standard follow-up will be required to determine calibration, reproducibility, diagnostic accuracy, and clinical utility.

Declarations

Funding
This work received no external funding. Development of STI and the J-Index was undertaken through ThermEval.

Data Availability
The examination records described in this manuscript are not publicly available because they derive from routine reading-service examinations and contain sensitive health information.

Ethics and Consent
This manuscript describes a methodological and analytical framework and does not report a prospective or retrospective human-subjects research cohort. Clinical images and information used for illustrative purposes were obtained during routine breast-thermography examinations and were deidentified for publication. Written informed consent for publication of the identifiable clinical information and associated images was obtained from the patient concerned. Figure 3 is an archival, fully deidentified thermographic image for which no patient-identifying information or linkage information is available.

Consent for Publication
Written informed consent for publication has been obtained for the identifiable clinical material presented in the manuscript. One additional archival thermographic image used solely to illustrate reconstruction morphology is fully deidentified, contains no patient-identifying information, and is no longer linkable to an identifiable individual.

Code Availability
The STI software and implementation-specific source code are proprietary and are not publicly available. The mathematical framework, analytical architecture, reconstruction principles, operational parameters, classification rules, figures, and representative outputs are described in the manuscript. Access to the proprietary implementation is restricted because the software is under active commercial development.

References

1. Sung H, Filho AM, Laversanne M, Ferlay J, Siegel RL, Soerjomataram I, et al. Global cancer statistics 2024: GLOBOCAN estimates of incidence and mortality worldwide for 34 cancers in 186 countries. *CA Cancer J Clin.* 2026;76(4):e70090. doi: 10.3322/caac.70090.

2. Harding C et al. Breast cancer screening, incidence, and mortality across US counties. *JAMA Internal Medicine*. 2015;175(9):1483–1489. doi:10.1001/jamainternmed.2015.3043.

3. Gimbrone MA Jr, Leapman SB, Cotran RS, Folkman J. Tumor dormancy in vivo by prevention of neovascularization. J Exp Med. 1972;136(2):261–276. doi:10.1084/jem.136.2.261.

4. Fang J, Yan L, Shing Y, Moses MA. HIF-1α-mediated up-regulation of vascular endothelial growth factor, independent of basic fibroblast growth factor, is important in the switch to the angiogenic phenotype during early tumorigenesis. *Cancer Res.* 2001;61(15):5731–5735.

5. Naumov GN, et al. A model of human tumor dormancy: an angiogenic switch from the nonangiogenic phenotype. J Natl Cancer Inst. 2006;98(5):316–325. doi:10.1093/jnci/djj068.

6. Konerding MA etal. Evidence for characteristic vascular patterns in solid tumors: Quantitative studies using corrosion casts. British Journal of Cancer. 1999;80(5-6):724.

7. Li C-Y et al. Initial Stages of Tumor Cell-induced Angiogenesis: Evaluation via Skin Window Chambers in Rodent Models. Journal of the National Cancer Institute. 2000;92(2):143-147. doi: 10.1093/jnci/92.2.143.

8. P. Henro et al, Breast microcalcifications: The lesions in anatomical pathology, Diagnostic and Interventional Imaging Volume 95, Issue 2, February 2014, Pages 141-152.

9. Naoto Nishida et al, Angiogenesis in Cancer, Vascular Health Risk Management, 2006 Sep; 2(3): 213–219, https://www.ncbi.nlm.nih.gov/pmc/articles/PMC1993983/.

10. Luo, Q et al. Vasculogenic mimicry in carcinogenesis and clinical applications. J Hematol Oncol 13, 19 (2020). doi: 10.1186/s13045-020-00858-6.

11. “Wavelet Transforms and Time-Frequency Signal Analysis;” Edited by Lokenath Debnath. https://link.springer.com/book/10.1007/978-1-4612-0137-3.

12. Ying-Ze Wang et al. Heat transport properties within living biological tissues with temperature-dependent thermal properties; https://iopscience.iop.org/article/10.1088/1674-1056/ac6b29.

13. R.K.Sahoo. Propagation of Thermal Waves with Lateral Heat Transfer. doi: 10.1016/0011-2275(94)90170-8.

14. P. Burgholzer et al; Three-dimensional Thermographic Imaging Using a Virtual Wave Concept, https://arxiv.org/ftp/arxiv/papers/1610/1610.00868.pdf.

15. Martin Zálešák et al. Solution approaches to inverse heat transfer problems with and without phase changes: A state-of-the-art review; https://www.sciencedirect.com/science/article/abs/pii/S0360544223013683.

16. Stanger L, Rockett T, Lyle A, Davies M, Anderson M, Todd I, et al. Reconstruction of microscopic thermal fields from oversampled infrared images in laser-based powder bed fusion. *Sensors (Basel).* 2021;21(14):4859. doi: 10.3390/s21144859.

17. Brown, B.S., et al. (2022). Influence of Thermal Diffusion on the Spatial Resolution of Thermal Imaging. https://par.nsf.gov/servlets/purl/10359552.

18. Zhang, H., et al. (2024). “Artificial intelligence-based classification of breast lesions from imaging data: Diagnostic accuracy and confidence measures.” https://pmc.ncbi.nlm.nih.gov/articles/PMC11093474/.

19. Moldovanu S, Munteanu D, Biswas KC, Moraru L. Breast lesion detection using weakly dependent customized features and machine learning models with explainable artificial intelligence. *J Imaging.* 2025;11(5):135. doi: 10.3390/jimaging11050135.

20. N. Weidner et al. “Current pathologic methods for measuring intratumoral microvessel density as a prognostic factor in breast Cancer" https://pubmed.ncbi.nlm.nih.gov/8534865/.

21. Rhif, M., et al. (2019). "Wavelet Transform Application for/in Non-Stationary Time-Series Analysis." https://www.mdpi.com/2076-3417/9/7/1345.

22. Hu, W., et al. (2016). "Multiple wavelet coherence for untangling scale-specific and localized features of transient processes." https://hess.copernicus.org/articles/20/3183/2016/hess-20-3183-2016.pdf.

23. Mallat SG. A theory for multiresolution signal decomposition: the wavelet representation. IEEE Trans Pattern Anal Mach Intell. 1989;11(7):674–693. doi:10.1109/34.192463.

24. Burnside ES, Rubin DL, Fine JP, Shachter RD, Sisney GA, Leung WK. Bayesian network to predict breast cancer risk of mammographic microcalcifications and reduce number of benign biopsy results: initial experience. Radiology. 2006;240(3):666–673. doi: 10.1148/radiol.2403051096.

25. Folkman, J. (1971). Tumor angiogenesis: therapeutic implications. New England Journal of Medicine, 285(21), 1182–1186. doi: 10.1056/NEJM197111182852108.

26. Anderson, A. R., & Chaplain, M. A. (1998). Continuous and discrete mathematical models of tumor-induced angiogenesis. Bulletin of Mathematical Biology, 60(5), 857–899. doi:.10.1006/bulm.1998.0042.

27. Metaxa L, Healy NA, O’Keeffe SA. Breast microcalcifications: the UK RCR 5-point breast imaging system or BI-RADS; which is the better predictor of malignancy? *Br J Radiol.* 2019;92(1103):20190177. doi: 10.1259/bjr.20190177.

28. Gautherie M, Gros CM. Breast thermography and cancer risk prediction. *Cancer.* 1980;45(1):51–56. doi: 10.1002/cncr.2820450110.